Model of Laminated Iron-Core Inductors for High Frequencies

Gabriele Grandi, *Member, IEEE*, Marian K. Kazimierczuk, *Senior Member, IEEE*, Antonio Massarini, *Member, IEEE*, Ugo Reggiani, *Member, IEEE*, and Giuseppe Sancineto

***Abstract*—We propose a model with frequency-dependent lumped parameters to represent the behavior of laminated iron-core inductors that are used in switching converters, i.e., for excitation frequencies above several kilohertz. The model applies to laminated iron cores with air gaps. We show that the core parameters can be calculated by using the same analytical expressions as those valid for gapless cores if a properly defined equivalent magnetic permeability is introduced instead of the iron sheet permeability. We compare the inductor model parameters calculated as functions of frequency with those obtained by measurements for two test inductors. The behavior of the inductors showed that the effects due to the eddy currents in the laminated iron core and the turn-to-turn and turn-to-core stray capacitances become significant in different frequency ranges.**

***Index Terms*—Coupling reactors, eddy currents, inductor high-frequency models, inductors, laminated iron magnetic cores, power filters, proximity effect, skin effect.**

NOMENCLATURE

$A_{\rm Fe}$	Iron core effective cross-sectional area.
$\hat{A}, \hat{B}, \hat{C}$	Complex integration constants.
C	Total parasitic capacitance.
f	Frequency.
f_r	Self-resonant frequency of the inductor.
f_{r1}	First self-resonant frequency of the inductor.
$\hat{H}_c$	Magnetic field intensity phasor inside a sheet.
$\hat{H}_{co}$	Magnetic field intensity phasor at the boundary of a sheet.
I_m	Inductor current amplitude.
$I_{m(Rc)}$	Current amplitude through R_c.
$\hat{I}$	Inductor current phasor.
$\hat{J}_y$	Phasor of the current density y component.
$\hat{k}_t$	Propagation constant.
$L_{\rm ac}$	Total inductance.
$L_{l({\rm ac})}$	AC winding leakage inductance.
$L_{m({\rm ac})}$	AC main inductance.
$L_{m({\rm dc})}$	DC main inductance.
L_s	Equivalent series inductance.
l_a, l_c	Air gap and iron sheet lengths.
N	Total number of turns.
N_l	Number of turn layers.
n	Number of core sheets.
$R_{\rm ac}$	Total ac resistance.
R_c	Core equivalent series resistance.
R_s	Equivalent series resistance.
R_w	AC winding resistance.
$R_{w({\rm dc})}$	DC winding resistance.
s	Lamination thickness.
$\hat{V}$	Phasor of the voltage induced across the winding.
X_s	Equivalent series reactance.
$\hat{Z}$	Inductor impedance.
δ_t, δ_w	Iron sheet and wire skin depths.
μ_o, μ_c	Vacuum and iron sheet permeabilities.
μ_e	Equivalent permeability.
μ_{rc}, μ_{rw}	Iron sheet and wire relative permeabilities.
μ_{rci}	Iron sheet initial relative permeability.
ρ_c, ρ_w	Iron sheet and wire electrical resistivities.
$\hat{\Phi}$	Magnetic flux phasor.
$\hat{\Phi}_c$	Phasor of the magnetic flux linking the coil.

Manuscript received December 11, 2002; revised April 9, 2004.

G. Grandi, U. Reggiani, and G. Sancineto are with the Department of Electrical Engineering, University of Bologna, I-40136 Bologna, Italy (e-mail: ugo.reggiani@mail.ing.unibo.it).

M. K. Kazimierczuk is with the Department of Electrical Engineering, Wright State University, Dayton, OH 45435 USA (e-mail: mkazim@cs.wright.edu).

A. Massarini is with the Department of Information Engineering, University of Modena and Reggio Emilia, I-41100 Modena, Italy (e-mail: massarini.antonio@unimore.it).

Digital Object Identifier 10.1109/TMAG.2004.830508

I. INTRODUCTION

LAMINATED iron-core inductors are widely used in power electronics applications. In particular, coupling reactors and filtering devices employ this type of inductor in the medium- to high-power range. In many power filtering devices, laminated iron-core inductors are preferred over both air-core and ferrite-core inductors. Air-core inductors are less expensive, but present larger sizes and higher copper losses. Furthermore, the leakage magnetic field presents a problem. The use of ferrite as a core medium offers some advantages, such as a lower copper loss compared to that of air-core inductors, and a lower core loss compared to that of laminated iron-core inductors. In addition, a low electrical conductivity limits the magnitude of eddy currents and allows ferrite to operate properly at frequencies up to several megahertz. On the other hand, the use of ferrite is limited to applications that require reduced core dimensions, such as small-signal high-frequency filters or small-inductance reactors. Ferrite is also quite expensive. Mainly for these reasons, the laminated iron-core inductors are widely employed in power filtering applications for excitation frequencies above several kilohertz. In particular, the possibility of geometrical arrangement of the sheets in several different ways leads to very flexible core constructions, capable of satisfying most of the inductor requirements.

A critical point in the design of laminated iron-core inductors is the evaluation of the inductance behavior versus frequency and the additional core losses. In spite of the core lamination, the effects produced by eddy currents due to the iron high electrical

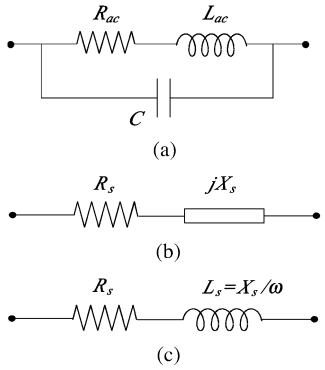

Fig. 1. Inductor models. (a) RLC equivalent circuit. (b) Series equivalent circuit. (c) Equivalent circuit measured by many impedance meters.

conductivity are significant, starting from frequencies of few tens of kilohertz.

In this paper, an analytical model of laminated iron-core inductors with air gaps is developed through a one-dimensional electromagnetic field analysis, taking into account eddy currents in the core. The magnetic permeability and electrical conductivity of iron are assumed to be independent of frequency. Linear media are assumed throughout the analysis, i.e., the magnetic field is low enough to avoid the iron core saturation. Therefore, the magnetic hysteresis of the core is also neglected. The proposed model considers the presence of air gaps in the magnetic circuit, as it is the case in most practical realizations of magnetic cores. The lumped parameter RLC circuit model shown in Fig. 1(a) is adopted to represent the frequency behavior of an inductor. The equivalent series resistance $R_{\rm ac}$ and inductance $L_{\rm ac}$ are frequency-dependent components due to skin and proximity effects in the winding [1] and eddy currents in the laminated iron core [2]. The parallel capacitance C models the turn-to-turn and turn-to-iron stray capacitances [3] and is assumed to be independent of frequency. Fig. 1(b) shows the series equivalent circuit of the inductor obtained from that depicted in Fig. 1(a). Fig. 1(c) shows the equivalent circuit used by most impedance meters.

II. Inductor Model

In the following sections, the inductor circuit models shown in Fig. 1 are discussed. The total ac resistance $R_{\rm ac}$, the total inductance $L_{\rm ac}$, and the overall stray capacitance C are described and estimated in detail. The total ac resistance $R_{\rm ac}$ can be written as $R_{\rm ac} = R_w + R_c$, where R_w is the ac winding resistance and R_c is the core equivalent series resistance. The total inductance $L_{\rm ac}$ is the sum of the main inductance $L_{m({\rm ac})}$ and the winding leakage inductance $L_{l({\rm ac})}$, i.e., $L_{\rm ac} = L_{m({\rm ac})} + L_{l({\rm ac})}$. In general, $R_w, R_c, L_{m({\rm ac})}$, and $L_{l({\rm ac})}$ are dependent on frequency f. To determine the behavior of these parameters as functions of frequency, models for both the winding and the laminated iron core are developed separately in Sections II-A and II-B, respectively. In Section II-C, the whole inductor model is considered including the parasitic capacitance, which is calculated on the basis of the inductor first self-resonant frequency.

A. Winding Model

The winding resistance of an inductor increases with frequency because of the skin and proximity effects. These effects are due to the time-varying electromagnetic field. The combined result of these two effects is a reduction in the effective cross-sectional area of the wire available for the current flow. Therefore, the ac winding resistance R_w at high frequencies becomes greater than the dc resistance $R_{w({\rm dc})}$. The ac winding resistance of an inductor with N_l layers was derived in [1] and simplified in [4] and [5] as

$$R_w = R_{w({\rm dc})} A \cdot \left[\frac{e^{2A} - e^{-2A} + 2\sin(2A)}{e^{2A} + e^{-2A} - 2\cos(2A)} + 2\frac{N_l^2 - 1}{3} \cdot \frac{e^{A} - e^{-A} - 2\sin A}{e^{A} + e^{-A} + 2\cos A} \right] \quad (1)$$

where A is a dimensionless quantity, which depends on the winding conductor geometry. The first and second terms in (1) represent the skin effect and the proximity effect contributions to the winding ac resistance, respectively. For a round wire of diameter d, the quantity $A = A_r$ is given by

$$A_r = \left(\frac{\pi}{4}\right)^{\frac{3}{4}} \frac{d}{\delta_w} \sqrt{\frac{d}{p}} \quad (2)$$

and for a strip wire of width a and height b, the quantity $A = A_s$ is described by

$$A_s = \frac{b}{\delta_w} \sqrt{\frac{a}{p}} \quad (3)$$

where p is the winding pitch, i.e., the distance between the centers of two adjacent conductors, and δ_w is the skin depth of the wire expressed as

$$\delta_w = \sqrt{\frac{\rho_w}{\pi \mu_o \mu_{rw} f}}. \quad (4)$$

In (4), $\mu_0 = 4\pi\ 10^{-7}$ H/m, μ_{rw} is the wire relative magnetic permeability, and ρ_w is the wire electrical resistivity. For a copper conductor, $\mu_{rw} = 1$ and $\rho_w = 17.24 \times 10^{-9}\ \Omega$·m at 20 °C.

The winding leakage inductance $L_{l({\rm ac})}$ was derived by Dowell [1] and simplified in [6] as

$$L_{l({\rm ac})} = R_{w({\rm dc})} \frac{A}{2\pi f} \cdot \left[\frac{e^{2A} - e^{-2A} - 2\sin(2A)}{e^{2A} + e^{-2A} - 2\cos(2A)} + 2\frac{N_l^2 - 1}{3} \cdot \frac{e^{A} - e^{-A} + 2\sin A}{e^{A} + e^{-A} + 2\cos A} \right]. \quad (5)$$

B. Core Model

Most inductors used in power electronics applications are realized with air gaps. In fact, the presence of an air gap is the most common way to linearize the behavior of an inductor over a large excursion range of the winding current, avoiding core saturation and reducing the harmonic distortion. Let us consider a laminated iron core with an air gap. Fig. 2 displays a rectilinear development of one of the sheets of the lamination packet, which forms the core. The inductor is composed of a core consisting of n sheets and N wire turns wound around it. In Fig. 2, s is the thickness of a single lamination, q is the width of the lamination, l_c is the axial length of the iron sheet, and l_a is the length of the air gap. The current $i(t)$ in the winding flows in the y direction

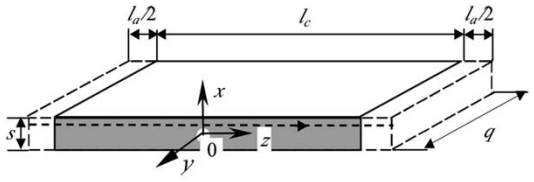

Fig. 2. Rectilinear development of a sheet.

of the Cartesian coordinate system shown in Fig. 2. Adopting a one-dimensional analysis, the magnetic field intensity vector in the core has only the component along the z axis, which depends on the x coordinate along the thickness and time t only. Similarly, the eddy current density vector has the y-directed component $J_y(x,t)$ only. The Ampère's circuital law is applied to a rectangular line consisting of a path located inside any sheet of the packet and the air gap (as indicated by the dashed line in Fig. 2) and of a path (not shown in Fig. 2) embracing the coil conductors in the region of space, where $x > 0$. We can write

$$H_c(x,t)l_c + H_a(x,t)l_a = Ni(t) + l_c \int_x^{s/2} J_y(x,t)\,dx \tag{6}$$

where $H_c(x,t)$ and $H_a(x,t)$ are the magnetic field intensities in the iron sheet and in its related air gap, respectively. As the total eddy current in any sheet is zero, only the eddy currents in the region between any x and $x = s/2$ of the considered sheet contribute to the circulation of the magnetic field intensity. The electrical parameters of a core with an air gap can be obtained through a one-dimensional analysis of the electromagnetic diffusion in a packet of laminations. The derivation of the impedance of nonsaturated laminated iron-core inductors operated under sinusoidal steady-state conditions is given in the Appendix. The derived expressions for the core equivalent series resistance R_c, related to the power loss due to eddy currents flowing in the core, and for the main inductance $L_{m(\mathrm{ac})}$, related to the magnetic field paths in the core, are given by

$$R_c = \omega L_{m(\mathrm{dc})} \frac{\delta_t}{s} \frac{\sinh\frac{s}{\delta_t} - \sin\frac{s}{\delta_t}}{\cosh\frac{s}{\delta_t} + \cos\frac{s}{\delta_t}} \tag{7}$$

$$L_{m(\mathrm{ac})} = L_{m(\mathrm{dc})} \frac{\delta_t}{s} \frac{\sinh\frac{s}{\delta_t} + \sin\frac{s}{\delta_t}}{\cosh\frac{s}{\delta_t} + \cos\frac{s}{\delta_t}} \tag{8}$$

where

$$\delta_t = \sqrt{\frac{\rho_c}{\pi\mu_e f}} \tag{9}$$

and

$$L_{m(\mathrm{dc})} = \mu_e N^2 A_{\mathrm{Fe}}/l_c \tag{10}$$

are the iron sheet skin depth, with ρ_c being the electrical resistivity of the iron sheet, and the dc and low-frequency main inductance, respectively. In (10), A_{Fe} is the effective cross-sectional area of the central limb. In (9) and (10), μ_e is the equivalent magnetic permeability defined by

$$\mu_e = \mu_c \frac{l_c}{l_c + \mu_{rc} l_a} \tag{11}$$

where $\mu_c = \mu_{rc}\mu_o$ is the absolute magnetic permeability and μ_{rc} is the relative magnetic permeability of the iron sheet. The permeability μ_e is defined so that a gapless magnetic core of length l_c and permeability μ_e is equivalent to the considered magnetic circuit with an air gap. From (11), it follows that for gapless iron cores $l_a = 0$, and the equivalent magnetic permeability μ_e equals the iron lamination permeability μ_c. In this case, (9) and (10) simplify to those given in [2].

C. Series Equivalent Circuit of Laminated Iron-Core Inductors

Fig. 1(b) depicts a series equivalent circuit of inductors, in which the equivalent series resistance R_s and reactance X_s are [4]

$$R_s = \frac{R_{\mathrm{ac}}}{(1-\omega^2 L_{\mathrm{ac}}C)^2 + (\omega C R_{\mathrm{ac}})^2} \tag{12}$$

$$X_s = \frac{\omega L_{\mathrm{ac}}\left(1 - \omega^2 L_{\mathrm{ac}}C - \frac{CR_{\mathrm{ac}}^2}{L_{\mathrm{ac}}}\right)}{(1-\omega^2 L_{\mathrm{ac}}C)^2 + (\omega C R_{\mathrm{ac}})^2} \tag{13}$$

with $\omega = 2\pi f$. Hence, the equivalent series inductance L_s is given by

$$L_s = \frac{X_s}{\omega}. \tag{14}$$

Most network analyzers and impedance meters display R_s and L_s. Fig. 1(c) shows the equivalent circuit measured by these meters.

A self-resonant frequency f_r of an inductor is defined as a frequency at which the reactance X_s becomes zero. Hence, the total parasitic capacitance C can be calculated from (13) using the measured first self-resonant frequency f_{r1} as

$$C = \frac{1}{(2\pi f_{r1})^2 L_{\mathrm{ac}}(f_{r1}) + \frac{R_{\mathrm{ac}}^2(f_{r1})}{L_{\mathrm{ac}}(f_{r1})}}. \tag{15}$$

The frequency f_{r1} is assumed to be a constant parameter in the whole operating frequency range of the inductor. The value of C was also verified by reactance measurements at frequencies much higher than the first self-resonance, where the capacitive branch becomes dominant with respect to the RL branch of Fig. 1(a).

III. Experimental Results

Measurements were carried out to test the validity of the proposed model for two laminated iron-core inductors with an air gap. An HP 4192A LF Impedance Analyzer (5 Hz–13 MHz) equipped with an HP 16047A test fixture [7] was employed to achieve a higher accuracy, minimizing residual parameters and contact resistances. The tested inductors were arranged by the same EI core depicted in Fig. 3 in order to emphasize the winding contribution. The value of the equivalent permeability of the EI core was calculated from (11) considering l_c as the length of the path comprised of the geometrical axis of the half central limb and that of one of the two outer limbs, and $l_a = 2l_{a1}$ as the total air gap. The parameters of interest for the two types of inductors are reported in Table I.

The magnetic permeability of the iron sheet used in the calculations corresponds to its initial value. The measured initial relative permeability was $\mu_{rci} = 300$. The measured resistivity of the iron sheet was $\rho_c = 7 \times 10^{-7}$ Ω·m. The lamination thickness was $s = 0.3$ mm. Figs. 4 and 5 show the measured

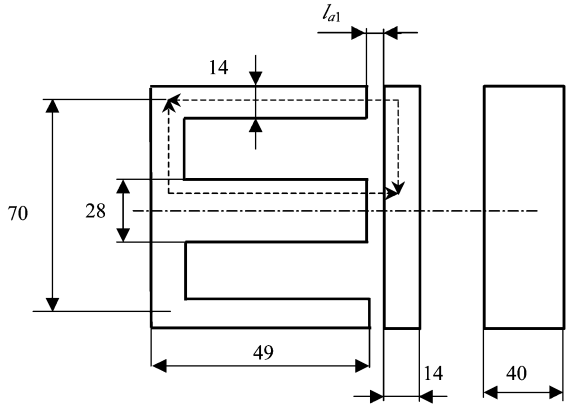

Fig. 3. EI core (dimensions in millimeters).

TABLE I
INDUCTOR PARAMETERS

Symbol	Quantity	Inductor #1	Inductor #2
d	wire diameter (mm)	1.5	1.46
p	winding pitch (mm)	$p \approx d$	$p \approx d$
N_l	number of turn layers	6	2
N_t	number of turns per layer	23	24
N	total number of turns	138	48
A_{Fe}	iron core cross-sectional area (mm^2)	1067	1067
l_c	length in the iron core (mm)	168	168
l_{a1}	width of each air gap (mm)	0.40	0.21
μ_e/μ_o	equivalent relative permeability	124	171
$L_{m(dc)}$	dc mean inductance (mH)	18.8	3.15
$R_{w(dc)}$	dc winding resistance (mΩ)	236	73
f_{r1}	first self-resonant frequency (MHz)	0.103	1.48
C	total parasitic capacitance (pF)	153	20.7

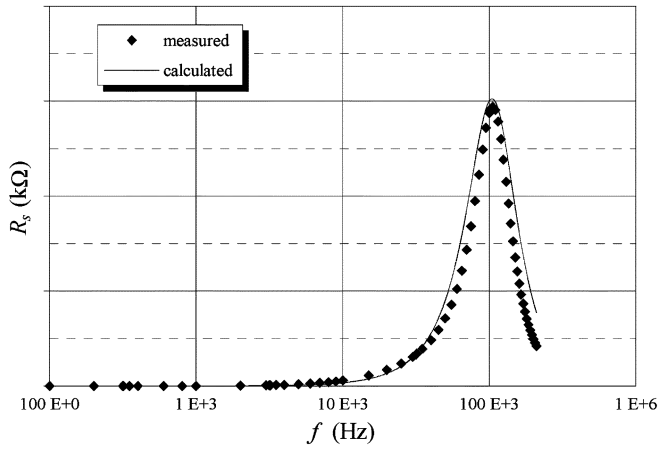

Fig. 4. Measured and calculated equivalent series resistance R_s, inductor #1.

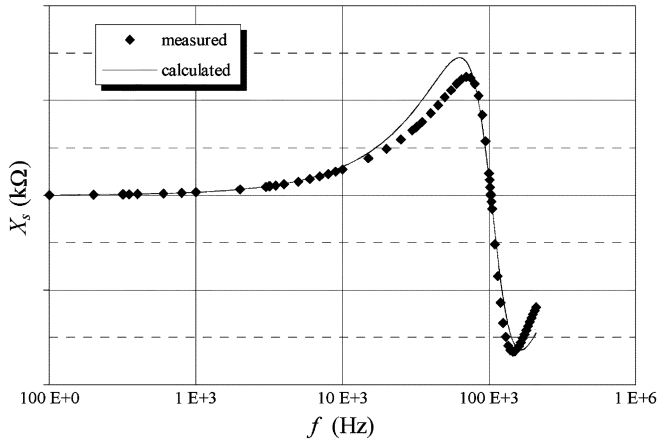

Fig. 5. Measured and calculated equivalent series reactance X_s, inductor #1.

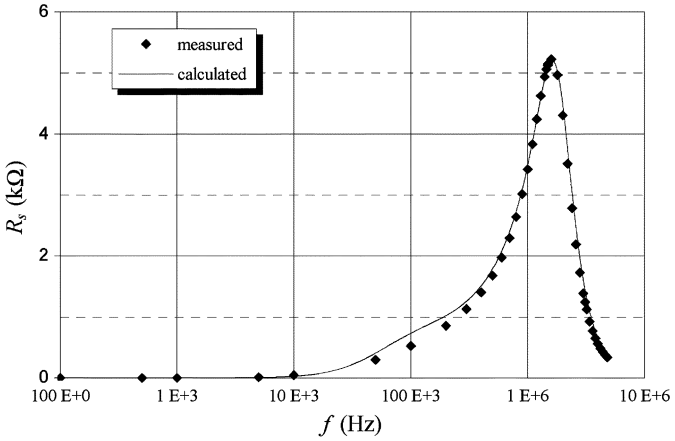

Fig. 6. Measured and calculated equivalent series resistance R_s, inductor #2.

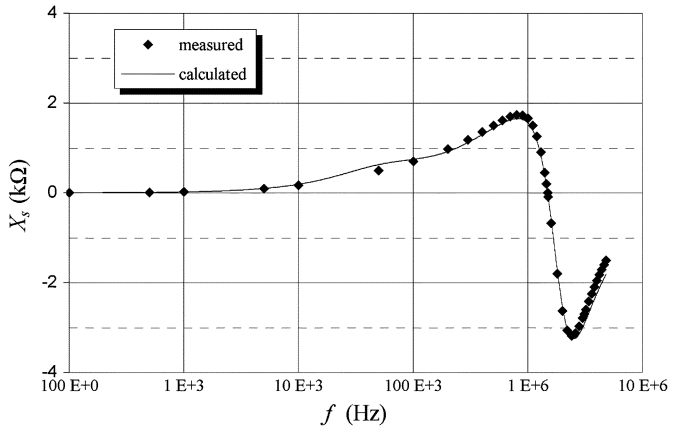

Fig. 7. Measured and calculated equivalent series reactance X_s, inductor #2.

(dots) and calculated (solid line) equivalent series resistance R_s and reactance X_s of the tested inductor #1 as functions of frequency, respectively. The measured (dots) and calculated (solid line) equivalent series resistance R_s and reactance X_s of the tested inductor #2 are depicted in Figs. 6 and 7, respectively. The measured first self-resonant frequency for the inductor #1 was $f_{r1} = 103$ kHz. The capacitance value calculated from (15) was $C = 153$ pF. In the case of the inductor #2, the first self-resonant frequency was $f_{r1} = 1.48$ MHz, resulting in a calculated value of capacitance $C = 20.7$ pF. The calculated capacitance value for the inductor #1, arranged with six layers, is greater than the one of the inductor #2 with two layers. The calculated capacitances indicate that the overall stray capacitance is lower if the inductor is arranged using a lower number of layers [8]. The proximity effect also gives a lower contribution to (1) and (5) for a lower number of layers. The figures reported here show that the obtained results are in good agreement with the measurements in the whole examined frequency range.

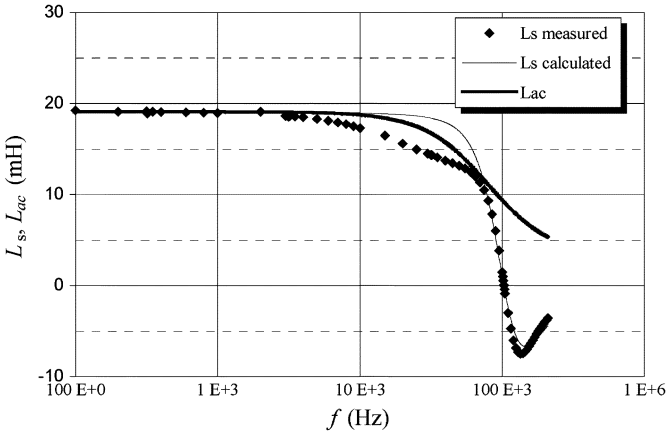

Fig. 8. Measured and calculated equivalent series inductance L_s and total inductance $L_{\rm ac}$, inductor #1.

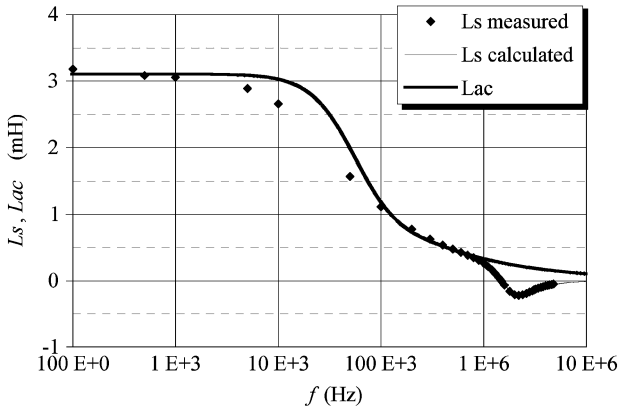

Fig. 9. Measured and calculated equivalent series inductance L_s and total inductance $L_{\rm ac}$, inductor #2.

At frequencies below the first resonance, the absolute value of the reactance of the parasitic capacitance is much higher than the impedance magnitude of the RL branch in Fig. 1(a), and resistances R_s and $R_{\rm ac}$ increase with frequency and remain close to each other. Therefore, the total power loss in the inductor (comprised of the core loss and the winding loss) increases with frequency at a fixed inductor current amplitude. At frequencies above the first resonance, the absolute value of the reactance of the parasitic capacitance is lower than the impedance magnitude of the RL branch, and the inductor current is partially shunted by the parasitic capacitance. Consequently, the total inductor power loss decreases with frequency at a fixed inductor current amplitude, and the equivalent series resistance R_s also decreases with frequency.

The behavior of the total inductance $L_{\rm ac}$ versus frequency deserves to be investigated. Fig. 8 depicts the total inductance $L_{\rm ac}$, and the measured and calculated equivalent series inductance L_s for the inductor #1. This figure indicates that the overall stray capacitance strongly affects the behavior of this inductor starting from about 80 kHz.

The total inductance $L_{\rm ac}$ and the measured and calculated equivalent series inductance L_s versus frequency for the inductor #2 are shown in Fig. 9. The curves of the calculated $L_{\rm ac}$ and L_s coincide up to 1 MHz and above that frequency they separate from each other. This means that the effect of the overall stray capacitance is almost negligible up to 1 MHz and, below that frequency, the decrease of the equivalent series inductance L_s can be attributed mainly to eddy currents, which reduce the magnetic field inside the core. Above that frequency, the equivalent series inductance L_s quickly decreases crossing the zero-axis due to the first parallel resonance and assuming negative value, i.e., the influence of the overall stray capacitance C becomes dominant.

The behavior of the examined inductors reveals that the effects due to the eddy currents in the laminated iron core and to the turn-to-turn and turn-to-core stray capacitances become significant in different frequency ranges. Below the first self-resonant frequency, the equivalent series inductance L_s practically coincides with the total inductance $L_{\rm ac}$. Then, it decreases with frequency compared to its dc value mainly because of the eddy currents produced in the laminated iron core, which expel the magnetic field out of the lamination. At frequencies above the first self-resonant frequency, the effect of the overall stray capacitance C becomes dominant.

IV. Conclusion

In this paper, an RLC model is proposed to represent the behavior of laminated iron-core inductors with air gaps for frequencies up to few megahertz. The total ac resistance and total inductance are frequency-dependent parameters because of the skin and proximity effects in the winding and the eddy currents in the laminated iron core. The hysteresis losses in the core are neglected. The eddy currents are evaluated by a one-dimensional field analysis considering nonsaturated iron cores. The overall stray capacitance, which models the turn-to-turn and turn-to-iron core stray capacitances, is calculated from the first self-resonant frequency of the coil and is assumed to be independent of frequency. The calculated results were in good agreement with the measurements carried out for two tested inductors. The presented model seems to be sufficiently accurate from zero to above the first self-resonant frequency of inductors. It can be used for computer-aided simulations of laminated iron-core inductors employed in high-frequency applications such as switching converters.

Appendix
Derivation of Impedance for Laminated Iron-Core Inductors With Air Gap

Starting from (6), it will be shown that (7) and (8) are valid for nonsaturated laminated iron cores with an air gap. With reference to Fig. 2, neglecting fringing effects in the air gap and taking into account the continuity of the magnetic flux density at the boundary between air and iron, it follows that

$$B_a(x,t) = B_c(x,t). \tag{A1}$$

Substituting (A1) into (6) and considering a linear constitutive law for the iron, we obtain

$$H_c(x,t)l_c = \frac{\mu_e}{\mu_c}N\left[i(t) + \frac{l_c}{N}\int_x^{s/2} J_y(x,t)\,dx\right], \quad -\frac{s}{2} < x < \frac{s}{2} \tag{A2}$$

where μ_e is given by (11). From (A2), we can write

$$\frac{\partial H_c(x,t)}{\partial x} = \frac{\mu_e}{\mu_c}\frac{\partial}{\partial x}\left[\int_x^{s/2} J_y(x,t)\,dx\right] = -\frac{\mu_e}{\mu_c}J_y(x,t). \quad \text{(A3)}$$

Faraday's law for the problem under consideration can be written as

$$\frac{\partial E_y(x,t)}{\partial x} = -\frac{\partial B_c(x,t)}{\partial t}. \quad \text{(A4)}$$

Applying Ohm's law $J_y = E_y/\rho_c$ and using (A3) and (A4), we can write

$$\frac{\partial^2 H_c(x,t)}{\partial x^2} = \frac{\mu_e}{\rho_c}\frac{\partial H_c(x,t)}{\partial t}. \quad \text{(A5)}$$

Introducing the magnetic field intensity phasor $\hat{H}_c(x)$ for sinusoidal steady state at angular frequency ω, (A5) becomes

$$\frac{d^2\hat{H}_c(x)}{dx^2} = \hat{k}_t^2\hat{H}_c(x) \quad \text{(A6)}$$

where

$$\hat{k}_t = \sqrt{\frac{j\omega\mu_e}{\rho_c}} = \frac{1+j}{\delta_t} \quad \text{(A7)}$$

and

$$\delta_t = \sqrt{\frac{\rho_c}{\pi\mu_e f}}. \quad \text{(A8)}$$

The differential equation (A6) has a general solution given by

$$\hat{H}_c(x) = \hat{A}e^{\hat{k}_t x} + \hat{B}e^{-\hat{k}_t x}. \quad \text{(A9)}$$

As the total eddy current in any sheet is zero, the magnetic field intensity in the considered sheet is not influenced by the remaining sheets and, because of symmetry, it satisfies the condition

$$\hat{H}_c(x) = \hat{H}_c(-x). \quad \text{(A10)}$$

Equation (A9) can then be written in the form

$$\hat{H}_c(x) = \hat{C}\cosh\hat{k}_t x. \quad \text{(A11)}$$

Applying the boundary conditions to (A11) yields

$$\hat{H}_c(x) = \hat{H}_{co}\frac{\cosh\left(\frac{1+j}{\delta_t}x\right)}{\cosh\left(\frac{1+j}{\delta_t}\frac{s}{2}\right)} \quad \text{(A12)}$$

where $\hat{H}_{co}$ is the magnetic field intensity phasor at the boundary of the sheet, i.e., for $x = \pm s/2$. In order to determine $\hat{H}_{co}$, the eddy-current density phasor $\hat{J}_y(x)$ in any sheet can be calculated using the differential form of the Maxwell–Faraday law. Neglecting the displacement current density in iron, which is much lower than the conduction current density, one obtains

$$\hat{J}_y(x) = (\nabla\times\hat{\mathbf{H}}_c(x))_y = -\hat{H}_{co}\left(\frac{1+j}{\delta_t}\right)\frac{\sinh\left(\frac{1+j}{\delta_t}x\right)}{\cosh\left(\frac{1+j}{\delta_t}\frac{s}{2}\right)}. \quad \text{(A13)}$$

From (A13), it follows that the phasor $\hat{J}_y(x)$ is an odd function of x

$$\hat{J}_y(x) = -\hat{J}_y(-x). \quad \text{(A14)}$$

Hence, (A2) written for $x = \pm s/2$ and in terms of phasors gives

$$\hat{H}_{co} = \frac{\mu_e}{\mu_c}\frac{N}{l_c}\hat{I} \quad \text{(A15)}$$

where $\hat{I}$ is the phasor of the sinusoidal current flowing through the coil. The magnetic flux phasor throughout a cross section of any sheet is calculated as

$$\hat{\Phi} = 2q\int_0^{s/2}\hat{B}_c(x)\,dx = 2q\mu_c\frac{\delta_t}{1+j}\tanh\left(\frac{1+j}{\delta_t}\frac{s}{2}\right)\hat{H}_{co} \quad \text{(A16)}$$

where q is the width of the sheet, as shown in Fig. 2.

Neglecting the leakage flux through the thin gaps between adjacent sheets, the magnetic flux linking the coil is

$$\hat{\Phi}_c = Nn\hat{\Phi} = 2N\mu_c D\frac{q}{s}\frac{\delta_t}{1+j}\tanh\left(\frac{1+j}{\delta_t}\frac{s}{2}\right)\hat{H}_{co} \quad \text{(A17)}$$

where N is the number of turns of the coil, n is the number of laminations in the packet, and $D = ns$ is the thickness of the packet. Substituting (A15) into (A17) yields

$$\hat{\Phi}_c = L_{m(\mathrm{dc})}\frac{\delta_t}{1+j}\frac{2}{s}\tanh\left(\frac{1+j}{\delta_t}\frac{s}{2}\right)\hat{I} \quad \text{(A18)}$$

where

$$L_{m(\mathrm{dc})} = \mu_e\frac{N^2Dq}{l_c} \quad \text{(A19)}$$

is the dc and low-frequency main inductance. Hence, the voltage induced across the winding by the magnetic flux is

$$\hat{V} = j\omega\hat{\Phi}_c = j\omega L_{m(\mathrm{dc})}\frac{\delta_t}{1+j}\frac{2}{s}\tanh\left(\frac{1+j}{\delta_t}\frac{s}{2}\right)\hat{I} \quad \text{(A20)}$$

and the impedance of the inductor is given by

$$\hat{Z} = \frac{\hat{V}}{\hat{I}} = j\omega L_{m(\mathrm{dc})}\frac{\delta_t}{1+j}\frac{2}{s}\tanh\left(\frac{1+j}{\delta_t}\frac{s}{2}\right). \quad \text{(A21)}$$

We can write (A21) as

$$\hat{Z} = \omega L_{m(\mathrm{dc})}\frac{\delta_t}{s}\left(\frac{\sinh\frac{s}{\delta_t}-\sin\frac{s}{\delta_t}}{\cosh\frac{s}{\delta_t}+\cos\frac{s}{\delta_t}} + j\frac{\sinh\frac{s}{\delta_t}+\sin\frac{s}{\delta_t}}{\cosh\frac{s}{\delta_t}+\cos\frac{s}{\delta_t}}\right). \quad \text{(A22)}$$

The real and imaginary parts of $\hat{Z}$ represent the core equivalent series resistance R_c (which accounts for the eddy-current loss in the core) and the coil main reactance $\omega L_{m(\mathrm{ac})}$, respectively. From (A21), these parameters are

$$R_c = \mathrm{Re}(\hat{Z}) = \omega L_{m(\mathrm{dc})}\frac{\delta_t}{s}\frac{\sinh\frac{s}{\delta_t}-\sin\frac{s}{\delta_t}}{\cosh\frac{s}{\delta_t}+\cos\frac{s}{\delta_t}} \quad \text{(A23)}$$

$$L_{m(\mathrm{ac})} = \frac{\mathrm{Im}(\hat{Z})}{\omega} = L_{m(\mathrm{dc})}\frac{\delta_t}{s}\frac{\sinh\frac{s}{\delta_t}+\sin\frac{s}{\delta_t}}{\cosh\frac{s}{\delta_t}+\cos\frac{s}{\delta_t}}. \quad \text{(A24)}$$

The expressions (A23) and (A24) for the core resistance R_c and main inductance $L_{m(\mathrm{ac})}$ are similar to those obtained in [2] for a gapless core inductor which use just the iron sheet permeability μ_c in (9) and (10). Hence, a laminated iron core with an air gap can be treated as a gapless one, when the equivalent permeability μ_e instead of μ_c is introduced. This substitution can be made also for the calculation of the time average power loss in the core $P_c = R_c I^2_{m(Rc)}/2$ using the core equivalent series resistance R_c, where $I_{m(Rc)}$ is the amplitude of the current through the core resistance R_c. In addition, it could be easily shown that the loss calculated from this expression coincides with that which can be obtained starting from the eddy-current density distribution and the power loss density distribution in a sheet of the packet [2], [9]. The total power loss in the inductor, comprised of the core loss and the winding loss, is $P_L = R_s I^2_m/2$, where I_m is the amplitude of the current through the inductor.

REFERENCES

[1] P. J. Dowell, "Effects of eddy currents in transformer windings," *Proc. Inst. Elect. Eng.*, vol. 113, pp. 1387–1394, Aug. 1966.

[2] J. Lammeraner and M. Stafl, *Eddy Currents*. London, U.K.: Iliffe Books, 1966.

[3] G. Grandi, A. Massarini, M. K. Kazimierczuk, and U. Reggiani, "Stray capacitances of single-layer solenoid air-core inductors," *IEEE Trans. Ind. Applicat.*, vol. 35, pp. 1162–1168, Sept. 1999.

[4] M. Bartoli, A. Reatti, and M. K. Kazimierczuk, "High-frequency models of ferrite core inductors," in *Proc. IEEE Int. Conf. Industrial Electronics, Control, Instrumentation, and Automation (IECON'94)*, Bologna, Italy, Sept. 5–9, 1994, pp. 1670–1675.

[5] ——, "Modeling iron-powder inductors at high-frequencies," in *Proc. IEEE Industry Applications Soc. Annu. Meeting*, Denver, CO, Oct. 2–7, 1994, pp. 1225–1232.

[6] M. K. Kazimierczuk, G. Sancineto, G. Grandi, U. Reggiani, and A. Massarini, "High-frequency small-signal model of ferrite core inductors," *IEEE Trans. Magn.*, vol. 35, pp. 4185–4191, Sept. 1999.

[7] *The Impedance Measurement Handbook*, Hewlett-Packard Co., 1989.

[8] A. Massarini and M. K. Kazimierczuk, "Self-capacitance of inductors," *IEEE Trans. Power Electron.*, vol. 12, pp. 671–676, July 1997.

[9] K. Howard and M. K. Kazimierczuk, "Eddy-current power loss in laminated iron cores," in *Proc. IEEE Int. Symp. Circuits and Systems (ISCAS'01)*, vol. III, Sydney, NSW, Australia, May 2001, pp. 668–671.

Gabriele Grandi (M'99) was born in Bologna, Italy, in 1965. He received the M.Sc. (cum laude) and Ph.D. degrees in electrical engineering from the Faculty of Engineering, University of Bologna, in 1990 and 1994, respectively.

In 1995, he joined the Department of Electrical Engineering, University of Bologna, as a Research Associate. Since 2000, he has been Lecturer of "Power Electronic Circuits," and since March 2003, he has qualified as Associate Professor. His research interests include modeling, simulation, and design of electronic power converters, with particular reference to power conditioning systems for renewable energy resources. Further topics of interest concern EMC problems related to switching converters and circuit models of HF components. He is author of about 50 papers published in technical journals and conference proceedings.

Marian K. Kazimierczuk (M'91–SM'91) received the M.S., and Ph.D., and D.Sci. degrees in electronics engineering from the Department of Electronics, Technical University of Warsaw, Warsaw, Poland, in 1971, 1978, and 1984, respectively.

He was a Teaching and Research Assistant from 1972 to 1978 and Assistant Professor from 1978 to 1984 with the Department of Electronics, Institute of Radio Electronics, Technical University of Warsaw. In 1984, he was a Project Engineer for Design Automation, Inc., Lexington, MA. In 1984-1985, he was a Visiting Professor with the Department of Electrical Engineering, Virginia Polytechnic Institute and State University, Blacksburg, VA. Since 1985, he has been with the Department of Electrical Engineering, Wright State University, Dayton, OH, where he is currently a Professor. His research interests are in resonant and PWM dc/dc power converters, dc/ac inverters, high-frequency rectifiers, electronic ballasts, magnetics, power semiconductor devices, and high-frequency high-efficiency power tuned amplifiers and lighting systems. He is the coauthor, with D. Czarkowski, of the book *Resonant Power Converters* (New York: Wiley, 1995). He has published over 130 technical papers, more than 60 of which have appeared in IEEE transactions and journals.

Dr. Kazimierczuk received the IEEE Harrell V. Noble Award for his contributions to the fields of aerospace, industrial, and power electronics in 1991. He is also a recipient of the 1991 Presidential Award for Faculty Excellence in Research, the 1993 College Teaching Award, the 1995 Presidential Award for Outstanding Faculty Member, and Brage Golding Distinguished Professor of Research Award from Wright State University. He was an Associate Editor of the IEEE TRANSACTIONS ON CIRCUITS AND SYSTEMS, I and serves as an Associate Editor for the JOURNAL OF CIRCUITS, SYSTEMS, AND COMPUTERS. He is a member of the Superconductivity Committee of the IEEE Power Electronics Society. He is a member of Tau Beta Pi.

Antonio Massarini (M'00) received the Laurea degree (cum laude) in nuclear engineering and the Ph.D. degree in electrical engineering from the University of Bologna, Bologna, Italy, in 1987 and 1992, respectively.

Since 1992, he has been a Teaching and Research Assistant with the Faculty of Engineering, Department of Engineering Sciences, University of Modena and Reggio Emilia, Modena, Italy. Since 2000, he has been an Associate Professor of Electrotechnics at the same University. He also cooperates with the Electrical Engineering Department of the University of Bologna, and was a Visiting Professor with the Department of Electrical Engineering, Wright State University, Dayton, OH. His research interests include MHD flow simulation, switched network simulation, magnetics, numerical methods for circuit analysis and design, and switching power converter simulation and design. More recently, his interests have also comprised EMC related problems.

Ugo Reggiani (M'92) received the Laurea degree (cum laude) in electrical engineering from the University of Bologna, Bologna, Italy, in 1969.

In 1971, he joined the Faculty of Engineering, University of Bologna, where he was Assistant until 1974 and Assistant Professor until 1980. Since 1980, he has been a Full Professor of Electrotechnics with the same Faculty. He was Head of both the Institute of Electrotechnics from 1989 to 1995, and the Department of Electrical Engineering from 1995 to 2001. He was coordinator of the Doctorate in Electrical Engineering at the University of Bologna from 1988 to 1998. He has been Chair of the Board of the professor of Electrical Engineering courses since 2002. Currently he is also Adjunct Professor at the University of Modena and Reggio Emilia. His main research interests concern electromagnetic field theory, electromechanical conversion, electromagnetic compatibility, modeling, and analysis of switched networks, and HF models of components.

Prof. Reggiani is a member of the IEEE Electromagnetic Compatibility Society and the Italian Electrotechnical and Electronics Association (AEI). He is a Registered Professional Engineer in Italy.

Giuseppe Sancineto was born in Crotone, Italy, in 1968. He received the M.Eng. and Ph.D. degrees in electrical engineering from the University of Bologna, Bologna, Italy, in 1998 and 2002, respectively.

In 1998, he was a visiting research scholar at Wright State University, Dayton, OH. He was a postdoctorate student at the Department of Electrical Engineering, University of Bologna, in 2002 and 2003. His research interests are in the field of power electronics, HF modeling of wound components, and renewable energy sources.